Neuron 49, 517–531, February 16, 2006 ©2006 Elsevier Inc. DOI 10.1016/j.neuron.2006.01.026

The HSPGs Syndecan and Dallylike Bind the Receptor Phosphatase LAR and Exert Distinct Effects on Synaptic Development

Karl G. Johnson,[1,5,6] Alan P. Tenney,[1,5] Aurnab Ghose,[1] April M. Duckworth,[1] Misao E. Higashi,[2] Karen Parfitt,[3] Oana Marcu,[4] Timothy R. Heslip,[4,7] J. Lawrence Marsh,[4] Thomas L. Schwarz,[2] John G. Flanagan,[1] and David Van Vactor[1,*]

[1] Department of Cell Biology and Program in Neuroscience
Harvard Medical School
240 Longwood Avenue
Boston, Massachusetts 02115

[2] Department of Neurobiology
Harvard Medical School and
Program in Neurobiology
Children's Hospital
300 Longwood Avenue
Boston, Massachusetts 02115

[3] Department of Biology and Program in Neuroscience
Pomona College
Claremont, California 91711

[4] Department of Developmental and Cell Biology and Developmental Biology Center
University of California, Irvine
Irvine, California 92697

Summary

The formation and plasticity of synaptic connections rely on regulatory interactions between pre- and postsynaptic cells. We show that the *Drosophila* heparan sulfate proteoglycans (HSPGs) Syndecan (Sdc) and Dallylike (Dlp) are synaptic proteins necessary to control distinct aspects of synaptic biology. Sdc promotes the growth of presynaptic terminals, whereas Dlp regulates active zone form and function. Both Sdc and Dlp bind at high affinity to the protein tyrosine phosphatase LAR, a conserved receptor that controls both NMJ growth and active zone morphogenesis. These data and double mutant assays showing a requirement of LAR for actions of both HSPGs lead to a model in which presynaptic LAR is under complex control, with Sdc promoting and Dlp inhibiting LAR in order to control synapse morphogenesis and function.

Introduction

The neuronal synapse is a specialized intercellular junction, the morphogenesis of which is vital for the function and plasticity of neural circuits. At the cell surface, multiple cell and substrate adhesion molecules work with each other and with extracellular matrix (ECM) proteins to maintain the physical bond between neuron and target and to regulate synapse form and function (reviewed by Yamagata et al. [2003]).

One class of ECM molecule particularly important for neuronal connectivity development is the heparan sulfate proteoglycans (HSPGs) (reviewed by Van Vactor et al. [2006] and Yamaguchi [2001]). Heparan sulfate (HS) is composed of a repeating dissaccaride unit (glucuronic acid and N-acetyl-glucosamine), which is then modified by deacetylation, epimerization, and sulfation to provide anionic binding sites for a number of extracellular partners (reviewed by Bernfield et al. [1999]).

Although the secreted HSPGs Agrin and Perlecan are well known as regulators of synapse assembly at the vertebrate neuromuscular junction, recent data suggest that cell surface HSPGs may also be important for synaptic development. Syndecan-2 localizes to multiple classes of synapses in the mammalian hippocampus (Hsueh and Sheng, 1999; Hsueh et al., 1998). Consistent with the synaptic accumulation of Syndecan-2, treatment of hippocampal tissue with heparinase to remove HS prevents efficient long-term potentiation (LTP) in CA1 pyramidal neurons, thus implicating HSPGs in synaptic plasticity (Lauri et al., 1999). Because LTP has been linked to morphological dynamics and maturation of the dendritic spines that process hippocampal inputs, it is particularly intriguing that misexpression of Syndecan-2 can induce accelerated morphological maturation of rat hippocampal dendritic spines in cell culture (Ethell and Yamaguchi, 1999). This suggests that Syndecan may play an important role in synaptic development and/or plasticity. However, in vivo elimination of Syndecan (or Syndecans) is needed to show the requirement of this HSPG family at the synapse.

Although the genetic analysis of Syndecan function in the mammalian central nervous system (CNS) is complicated by the existence of several family members, a single Syndecan gene (*Sdc*) is present in *Drosophila* (Spring et al., 1994). Analysis of Sdc function in *Drosophila* has highlighted roles in axonal pathfinding (Johnson et al., 2004; Rawson et al., 2005; Steigemann et al., 2004; Fox and Zinn, 2005); however, the function of Sdc at the synapse is unknown. By far the best-characterized *Drosophila* synapse is the larval NMJ. Unlike vertebrate and *C. elegans* NMJs, the *Drosophila* counterpart is glutamatergic, analogous to the majority of mammalian CNS excitatory synapses (Gramates and Budnik, 1999). By larval hatching, nascent NMJs have formed in the periphery that will grow extensively throughout larval life (see Figure 1A for a schematic of ventral muscles and motor nerves). At the latest stage of larval development (third instar), presynaptic arbors fan out extending multiple branches decorated with many round synaptic varicosities ("boutons") that contain the active zones that organize glutamate release (Figure 1B).

Another class of cell surface molecules involved in synapse development is the receptor protein tyrosine phosphatases (RPTPs) (reviewed by Johnson and Van Vactor [2003]). LAR family RPTPs have been identified

*Correspondence: davie@hms.harvard.edu

[5] These authors contributed equally to this work.

[6] Present address: Department of Biology and Program in Neuroscience, Pomona College, Claremont, California 91711.

[7] Present address: NemaRx Pharmaceuticals Inc., #4, 3535 Research Rd. NW, Calgary Alberta, Canada T2L 2K8.

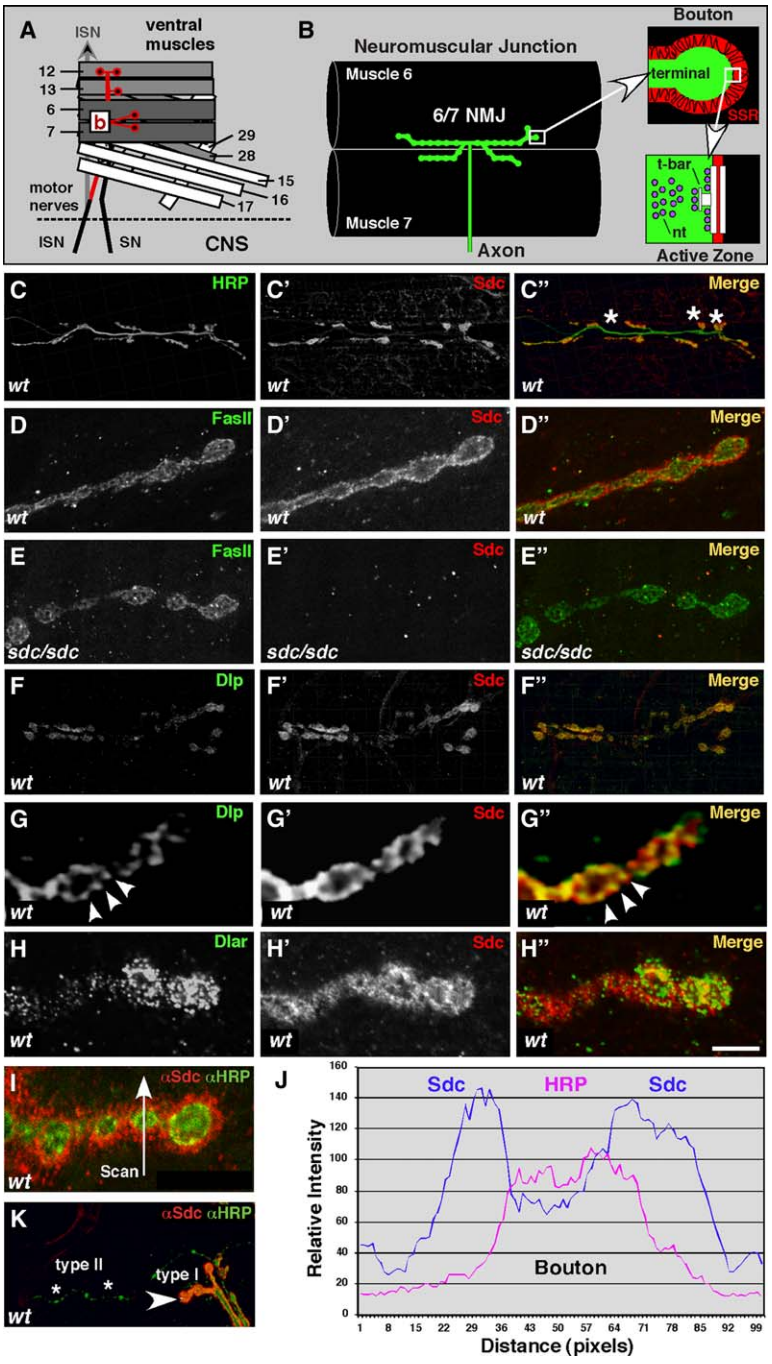

Figure 1. Syndecan Localizes to the *Drosophila* Neuromuscular Junction

(A and B) Diagrams of the ventral body-wall muscles (numbered) and motor nerves from the dorsal aspect of the *Drosophila* larva (A) and the 6/7 neuromuscular junction (B). The intersegmantal nerve b (red) projects to the ventral longitudinal muscle group (gray); muscles 6 and 7 (dark gray) are part of this group and are dually innervated by the most proximal branch (b). An individual synaptic bouton showing the location of the subsynaptic reticulum (SSR) and a representation of the active zone are shown at right.

(C) Immunostaining with anti-HRP and anti-Sdc antibodies at the 6/7 NMJ. Sdc is highly concentrated at synaptic boutons (asterisks in merge).

(D) Higher magnification shows that the majority of Sdc appears to exist in a halo surrounding FasII.

(E) Sdc mutant larvae (Sdc^{P}/*Df48,ubi-sara*) lack all detectable Sdc staining at the 6/7 NMJ.

(F) Dlp and Sdc immunoreactivity show high degrees of overlap within NMJs at the muscle 6/7 cleft.

(G) Higher magnification images of terminal boutons show that Dlp localizes to punctate structures that are contained within the broader Sdc distribution (arrowheads).

(H) *Drosophila* LAR (Dlar) localizes preferentially to terminal boutons (D) and shows a high degree of overlap with Sdc at the 6/7 NMJ.

(I and J) A single plane of optical section from the confocal microscope allowed a linescan (white line) of relative fluorescence intensity to compare the Sdc and HRP epitopes. A plot of the intensity data as a function of position is shown in (J).

(K) Immunostaining with anti-Sdc and anti-FasII antibodies to the NMJ on muscles 12 and 13 shows that Sdc localizes preferentially to type Is and Ib boutons (arrowhead) but is absent from type II boutons (asterisks). Scale bar in (E) represents 50 μm for (C), 5 μm for (D) and (E), and 3 μm for (F).

with roles in synapse formation in *Drosophila* (Kaufmann et al., 2002), *C. elegans* (Ackley et al., 2005), and vertebrates (Dunah et al., 2005). Although relatively few RPTP-ligand interactions have been tested for function in vivo, several molecules have been identified that bind to LAR-family receptors, including Laminin-Nidogen complexes and HSPGs. Although genetic data implicate Nidogen in the synaptic LAR pathway of *C. elegans* (Ackley et al., 2005), synaptic HSPG-LAR interactions have not been tested in any organism.

In this study, we examine the synaptic functions of two HSPGs in *Drosophila*: Syndecan (Sdc) and the glycosylphosphatidyl-inositol (GPI) anchored glypican Dallylike (Dlp). We find that Sdc is required for normal levels of morphological growth at the larval NMJ without obvious effects on the electrophysiology of the synapse. In contrast, Dlp is necessary to regulate the form and physiological function of active zones but plays no apparent role in regulation of bouton addition. Becuase LAR-family receptor protein tyrosine phosphatases have been shown to bind HSPGs in different contexts (Aricescu et al., 2002; Fox and Zinn, 2005), and because LAR regulates both NMJ growth and active zone structure in *Drosophila* (Kaufmann et al., 2002), we asked if Sdc and Dlp might function through interactions with LAR. We find that both Sdc and Dlp bind to *Drosophila* LAR

at high affinity. Moreover, multiple double mutant experiments indicate that both Sdc and Dlp act upstream of LAR. Our results reveal a complex regulatory relationship between LAR and two HSPGs that control distinct aspects of synapse biology, with Sdc acting to promote LAR function and NMJ growth, and Dlp acting to antagonize LAR function and influence active zone structure and physiology.

Results

Drosophila HSPGs Localize to the Neuromuscular Junction

Syndecan-family HSPGs have been localized to vertebrate glutamatergic synapses (Hsueh and Sheng, 1999; Hsueh et al., 1998); however, Sdc distribution at analogous synapses in *Drosophila* was unknown. Using confocal microscopy, we examined wild-type third instar larval fillets and compared the staining patterns of antibodies against *Drosophila* Sdc, the presynaptic membrane marker horseradish peroxidase (αHRP), and the cell adhesion molecule Fasciclin II (αFasII). The localization of Sdc is quite specific to the synapse, with little or no protein detected along motor axons or branches that are free of boutons (Figures 1C and 1D), despite abundant accumulation along motor axons at early stages of development (Johnson et al., 2004). To confirm the specificity of the Sdc staining at the NMJ, we examined *Sdc* mutant larvae ($Sdc^{I(2)10608}/Df[2R]48$, *ubi-sara*; see Experimental Procedures) and no Sdc signal was detected (Figure 1E).

Inspection of wild-type NMJs revealed that Sdc staining extends in a halo-like distribution around type Ib and Is boutons (Figures 1D and 1I). This pattern indicates that the majority of synaptic Sdc is found either on the muscle surface or in the space between the presynaptic membrane and the subsynaptic reticulum (SSR) (see Figure 1B). To examine Sdc distribution more thoroughly, we performed line scans of fluorescence intensity comparing the Sdc signal to that of the HRP epitope (Figure 1J). Although Sdc and HRP show some overlap, most of the Sdc surrounds the bouton. Sdc is absent from type II boutons that lack SSR structures (e.g., on muscles 12 and 13; Figure 1H).

Although anti-Dlp antibodies have been used to characterize Dlp localization during epitheilial patterning and axon guidance (Johnson et al., 2004; Kirkpatrick et al., 2004; Rawson et al., 2005), the synaptic localization of glypicans have not been described in any organism. The localization of Dlp and Sdc overlapped at the NMJ (Figure 1F). Like Sdc, very little Dlp was found along motor axons or bouton-free regions of the presynaptic arbor. Careful examination revealed that Dlp accumulates in punctate structures that are contained within a broader distribution of Sdc (Figure 1G, arrowheads), suggesting that Dlp is restricted to a subset of synaptic space.

Syndecan Is Required to Promote Normal Synapse Growth

Given the synaptic localization of Sdc and Dlp, we wondered if they might be required for some aspect of synaptogenesis. After first ruling out defects in embryonic motor axon guidance in both *Sdc* and *Dlp* zygotic loss-of-function (LOF) mutants (see Supplemental Data), we examined larval NMJs with several anatomical markers. Using the presynaptic markers HRP and MAP1b/Futsch, we compared several wild-type strains with mutants lacking Sdc or Dlp. No gross defects in the branched structure of presynaptic terminals were observed (Figures 2A–2C). For a more detailed view of synapse structure, we examined a series of additional markers, including the presynaptic active zone antigen NC82, the SSR marker Dlg, and glutamate receptors (GluRIII) that cluster on the postsynaptic membrane. No obvious defects in the levels or distribution of these markers were observed in *Sdc* mutants (Figures 2D–2G). We also found no defects in levels or localization of the synaptic vesicle markers Synaptotagmin (Syt) and Cysteine-string protein (CSP), or the endocytic marker Endophillin (not shown). Similar results were obtained for *Dlp* mutants with HRP, Futsch, FasII, NC82, GluRIII, Sdc, and LAR as markers (not shown).

Although we found no alteration in the distributions of synaptic marker proteins in *Sdc* mutants, we did discover a defect in synaptic growth. At the crawling third instar stage, wild-type NMJs contain a stereotyped, segment-specific number of boutons reflecting the steady growth of the synapse over larval life. When we quantified bouton number at NMJs formed on muscles 7 and 6 in a wild-type strain (Canton S) and in different *Sdc* alleles, we found a highly significant reduction in bouton number (over 35% in $Sdc^{I(2)10608}/Df48$,*ubi-Sara*, $p < 10^{-8}$) (Figure 2H, triple asterisk); comparable phenotypes were observed at abdominal segments A2 and A3 (not shown). When wild-type was compared to a control genotype with normal levels of Sdc and a genetic background identical to the *Sdc* mutant strain, no significant difference was found (*P12357*/*P12345*) (Figure 2H). We used mitotic recombination as an additional control for genetic background effects to remove flanking polymorphisms from the *Sdc* chromosome, and the NMJ phenotype of the recombinant was not significantly less severe than the original *Sdc* mutant ($p = 0.2$) (Figure 2H). To be certain that this *Sdc* phenotype did not reflect reduction in the overall growth of *Sdc* mutant tissues, we compared the size of muscles 6 and 7 in mutants and controls but found no significant difference (mean muscle areas were 79698 μm^2 in wild-type compared to 78702 μm^2 in *Sdc* mutants; $p = 0.8$). Thus, we concluded that Sdc is required for the normal addition of boutons throughout NMJ growth.

We next asked if we could rescue the *Sdc* NMJ phenotype with a cDNA transgene under the control of a tissue-specific GAL4 driver. We found that expression of an Sdc construct under control of a presynaptic driver (elav-GAL4) provided nearly complete rescue of the NMJ growth defect ($p < 10^{-4}$) (Figure 2H, double asterisk). The localization of the UAS-Sdc transgenic protein (driven by elav-GAL4 in an *Sdc* LOF background) was indistinguishable from the pattern of endogenous Sdc in wild-type (Figure 2J). When we used a postsynaptic driver (24B-GAL4) to express the same UAS-Sdc transgene, we found only a very weak rescue activity (15.5% recovery) (Figure 2H, single asterisk), suggesting that Sdc acts primarily on the presynaptic membrane.

As a test of Sdc specificity at the NMJ, we examined synapses lacking Dlp. Interestingly, the number of

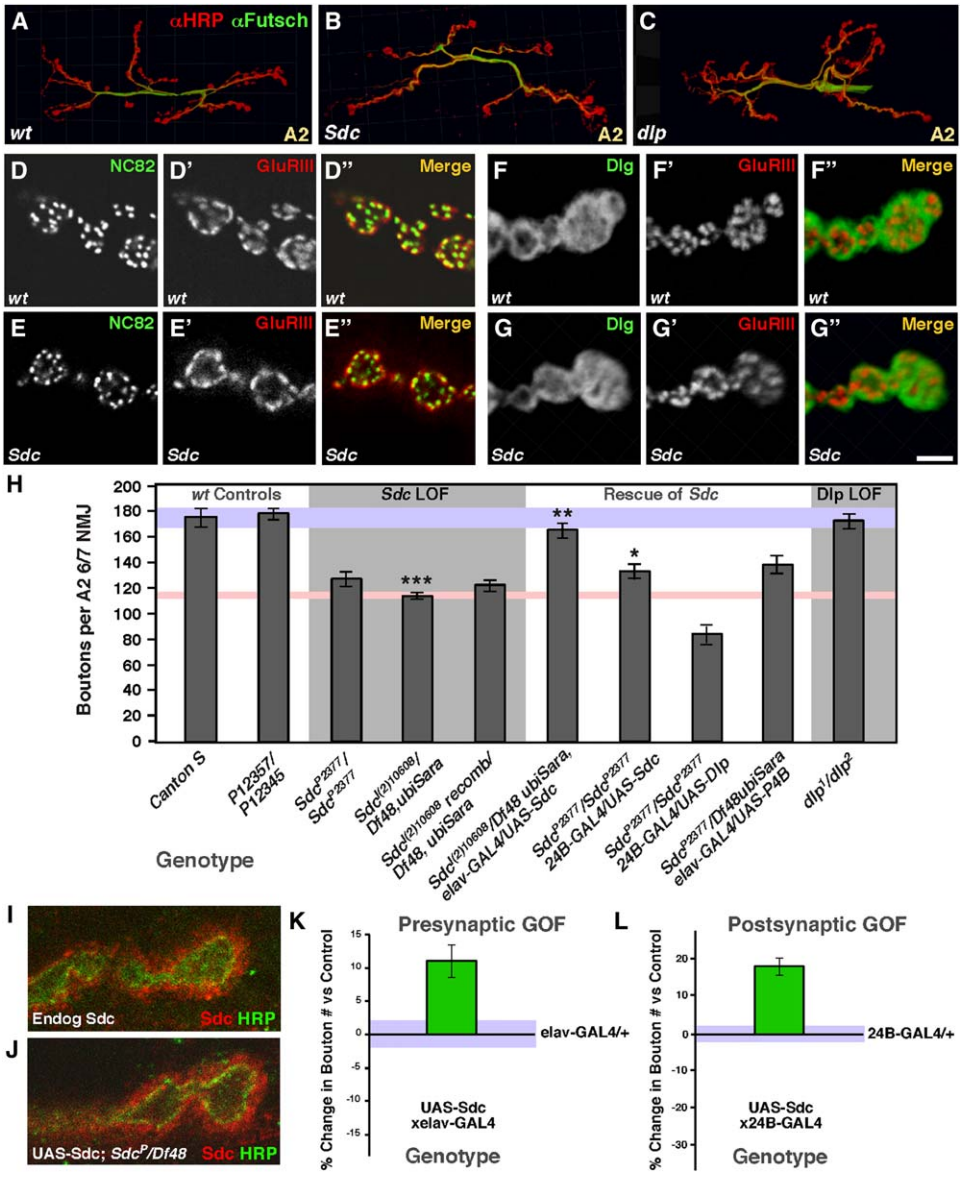

Figure 2. Syndecan Is Required to Promote Synapse Growth

(A–C) Confocal z projections of the 6/7 cleft in wild-type (A), a $Sdc^{P}/Df48,ubi\text{-}sara$ mutant (B), and a dlp^{1}/dlp^{2} mutant (C) from larvae stained with anti-HRP and anti-Futsch show no gross defects in the overall NMJ structure.

(D and E) $Sdc^{P}/Df48,ubi\text{-}sara$ mutant NMJs (E) exhibit no obvious defects in NC82-antigen or GluRIII expression or in GluRIII clustering around NC82-positive active zones, compared to wild-type (D).

(F and G) The distrubution of the SSR marker Dlg also appeared normal in $Sdc^{P}/Df48,ubi\text{-}sara$ mutant NMJs (G) compared to wild-type (F).

(H) Quantification of bouton numbers per 6/7 NMJ (segment A2) shows that Sdc^{P2377}/Sdc^{P2377}, $Sdc^{l(2)10608}/Df48,ubi\text{-}sara$ mutants ($p = 9.5 \times 10^{-9}$; triple asterisk) or a recombinant *Sdc* chromosome (Sdc^{P} *recomb*$/Df48,ubi\text{-}sara$ mutants) have significantly fewer boutons compared to Canton S or a genetically matched wild-type control (P12357/P12345). Presynaptic expression of UAS-Sdc rescues the bouton reduction phenotype ($p = 2.3 \times 10^{-5}$; double asterisk), whereas postsynaptic expression provides only limited rescue (single asterisk). UAS-Dlp is unable to rescue the *Sdc* phenotype, and mutations in *dallylike* (dlp^{1}/dlp^{2}) do not cause a significant reduction in bouton number. Blue bar represents SEM of Canton S, and pink bar represents SEM of $Sdc^{P}/Df48,ubisara$.

(I and J) Sdc distribution in an *Sdc* mutant expressing UAS-Sdc under a neuron-specific elav-GAL4 source ([K], also used for rescue in [H]) is equivalent to wild-type (J).

(K and L) Elevated expression of UAS-Sdc (GOF) in wild-type larvae under either presynaptic elav-GAL4 (L) or postsynaptic 24B-GAL4 both induce a significant percentage increase in bouton number compared to GAL4 alone (blue bars represent SEMs of GAL4 alone control values). Scale bar represents approximately 50 μm in (A)–(C), 4 μm in (D)–(G), and 2 μm in (J) and (K).

boutons in the *dlp* mutant were within normal range (Figure 2H). In the embryonic CNS, we previously found that elevation of Dlp expression can rescue some of the midline axon guidance defects seen in *Sdc* mutants (Johnson et al., 2004), suggesting functional redundancy between the two HSPGs. As a further test of specificity at the synapse, we expressed wild-type Dlp in the *Sdc* mutant but found no rescue of the growth defect

(Figure 2H). Interestingly, elevation of Dlp enhanced the *Sdc* phenotype, suggesting that there might be an antagonistic relationship between the two HSPGs. Thus, in the context of synapse growth, Sdc function appears to be highly specific compared to Dlp.

In cell culture, elevated expression of vertebrate Syndecan-2 can accelerate the maturation of glutamatergic synapses (Ethell and Yamaguchi, 1999), suggesting that HSPG levels may be instructive for synapse growth. To ask if Sdc can achieve this effect in vivo, we tested whether Sdc is limiting for NMJ growth in *Drosophila*. Using GAL4 drivers specific to neurons or muscle cells, we misexpressed Sdc in a wild-type background. Presynaptic elevation of Sdc increased bouton number compared to GAL4 alone ($p < 0.001$) (Figure 2K). Interestingly, despite the poor rescue activity of postsynaptic Sdc, muscle expression of Sdc in a wild-type background gave a similar increase in synapse size ($p < 0.001$) (Figure 2K). This gain-of-function (GOF) phenotype was the opposite of that observed in the Sdc LOF, demonstrating that Sdc is limiting for synapse growth.

Dallylike Regulates Synaptic Transmission and Active Zone Morphology

Cell surface HSPGs have been implicated as regulators of synaptic function by gross enzymatic depletion of HS (e.g., Lauri et al. [1999]). To test if specific HSPGs are indeed required for normal synapse physiology, we measured the excitatory junctional potential (EJP) elicited by stimulation of the intersegmental motor nerve trunk in crawling third instar larvae at 1.0 mM extracellular Ca^{2+}, comparing a wild-type strain (Oregon R, OR) to a strong *Sdc* LOF genotype ($Sdc^{l(2)10608}/Df[2R]48,ubi\text{-}sara$) (Figures 3A and 3B). Compared to controls, *Sdc* mutant EJPs were not significantly reduced ($p = 0.9$) (Figures 3A, 3B, and 3D). We also measured the amplitude and frequency of spontaneous release events (miniature events; mEJPs); although there seemed to be a slight decrease relative to OR, it was not statistically significant ($p = 0.8$ and 0.6, respectively) (Figures 3E and 3F). This suggests that *Sdc* mutant NMJs accomplish some type of functional compensation for their decreased overall size.

We next examined the physiology of *dlp* mutants. Here, we found a significant increase in EJP amplitude (45% higher than OR in dlp^1/dlp^2, $p = 0.0001$) (Figures 3C and 3D), without a significant change in muscle input resistance. Comparable EJP amplitudes were seen when the dlp^1 allele was examined over a deletion at the locus (not shown). To confirm that loss of Dlp alone induced the change in EJP amplitude, we also performed a rescue experiment with a full-length wild-type UAS-Dlp transgene; the wild-type Dlp transgene restored EJP values to normal levels ($UAS\text{-}Dlp[+];dlp^1/dlp^2$ EJPs were 32.4 mV [n = 9] compared to 32.5 mV observed in OR [n = 8]; $p = 0.98$). Similar to Dlp function during axon guidance (Rawson et al., 2005), GAL4 activity was not required to achieve full rescue of the *dlp* synapse phenotype, suggesting that very small quantities of Dlp are sufficient to restore synaptic function.

The *dlp* neurotransmission phenotype could reflect increased glutamate release or elevated postsynaptic sensitivity. To distinguish between these possibilities, we analyzed mEJPs. The mean amplitude of *dlp* mutant mEJPs was not significantly different from wild-type ($p = 0.2$) (Figure 3E). The frequency of mEJPs was also normal in *dlp* mutants ($p = 0.5$) (Figure 3F), suggesting that the defect was specific to the evoked release mechanism. To compare the number of glutamate quanta released with each presynaptic stimulus, we calculated quantal content values with mEJP amplitude to determine quantal size correcting for nonlinear summation and found a significant increase in *dlp* mutants relative to wild-type (64%, $p = 0.0002$) (Figure 3G). Thus, in contrast to Sdc, Dlp is required for normal synapse physiology, acting to restrict the number of quanta released per stimulus.

Neurotransmitter release is orchestrated at special sites on the presynaptic membrane called active zones (AZs) that can be visualized at an ultrastructural level. We asked if there might be a morphological correlate to the functional defects observed in *dlp* mutants. Serial section transmission electron microscopy (EM) was performed for *dlp*, *Sdc*, and a wild-type strain; multiple type Ib boutons from several animals were examined for each genotype. We found no gross alteration in overall NMJ structure. Key structures such as the subsynaptic reticulum (SSR), synaptic vesicles, AZs, and t bars were present in both HSPG mutants (Figures 3H–3P).

To obtain a quantitative metric of AZ structure, we measured the dimensions of AZs in the HSPG mutants. In *Sdc* mutants, there was no significant change in AZ area relative to controls ($p = 0.7$) (Figure 3Q), consistent with the absence of a physiological phenotype. However, *dlp* mutant AZs were significantly smaller than wild-type or *Sdc* ($p = 0.02$) (Figure 3Q). A decrease in AZ area alone could not explain the increased quantal context in *dlp* mutants, so we counted the number of AZs per bouton and found that although *Sdc* mutants are not significantly different from control, *dlp* mutants show a roughly 2-fold increase in AZ density (Figure 3R). Finally, we asked if Dlp is limiting for AZ morphogenesis. EM reconstruction after postsynaptic elevation of UAS-Dlp revealed a nearly 2-fold increase in AZ area, precisely the opposite of *dlp* loss of function (Figure 3S). Together with our analysis of NMJ growth, the physiological and ultrastructural data reveal striking specificity in HSPG action at the synapse, with Sdc controlling NMJ growth and Dlp controlling AZ morphogenesis.

Sdc and Dlp Bind to LAR

Among candidate receptors that might mediate the synaptic effects of HSPGs, the LAR family of receptor protein tyrosine phosphatases (RPTPs) was particularly attractive because the LAR ortholog PTP-σ binds to two vertebrate proteoglycans, Agrin and Collagen XVIII (Aricescu et al., 2002), and LAR is required for synapse growth as well active zone form and function in *Drosophila* (Kaufmann et al., 2002). Moreover, while this manuscript was in review, binding between LAR and Sdc was described in the *Drosophila* embryo (K. Zinn, personal communication; Fox and Zinn, 2005).

To test for a cell-surface interaction between LAR and Sdc, we constructed a fusion protein with the *Drosophila* Sdc extracellular (EC) domain linked to an alkaline phosphatase (AP) tag and used it to probe *Drosophila* S2 cells expressing a cDNA encoding an epitope-tagged

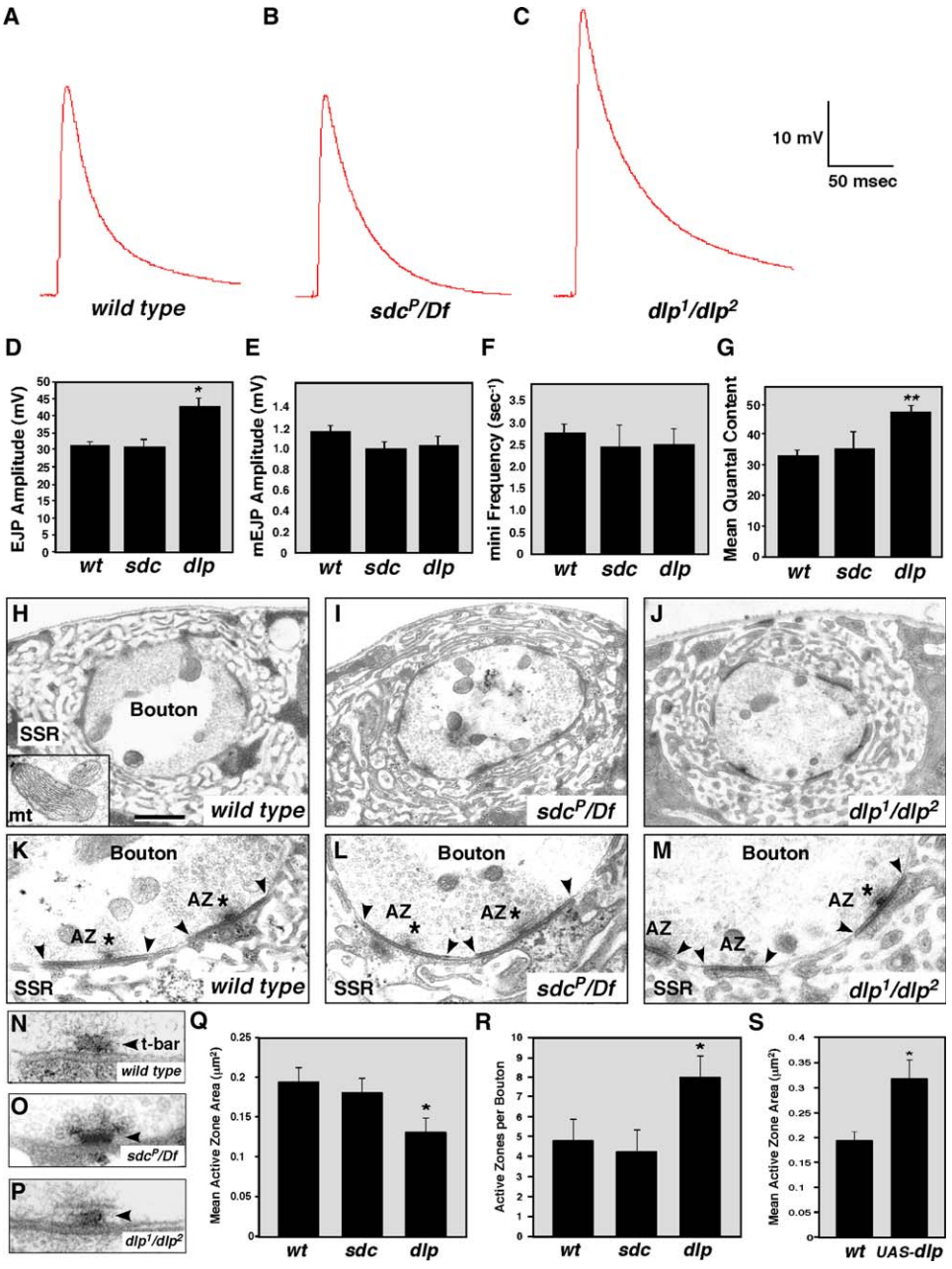

Figure 3. Dallylike Controls Neurotransmission and Active Zone Structure

(A–C) Evoked EPSPs recorded in muscle 6 of wild-type (A), *Sdc* (*Sdc*$^{I(2)10608}$*/Df[2R]48, ubi-sara,* [B]), and *dlp* (*dlp*^{1}*/dlp*^{2}, [C]) genotypes show that *dlp* mutants have increased responses to identical stimuli (see Experimental Procedures).

(D) Quantitative histograms show that *dlp* mutant EPSPs are 35% higher than Oregon R or *Sdc* mutants (p = 0.001, asterisk).

(E and F) Histograms compare miniature EPSP amplitude (E) and frequency (F); these differences are not statistically significant (see text).

(G) Calculation of quantal content values (corrected for nonlinear summation) for Oregon R (wt), *Sdc*^{P}*/Df48,ubi-sara*, and *dlp*^{1}*/dlp*^{2} reveals a highly significant increase in *dlp* mutants (45%, p = 0.0001; double asterisk). Uncorrected values for Oregon R, *Sdc*^{P}*/Df48,ubi-sara*, and *dlp*^{1}*/dlp*^{2} are 30.40 ± 1.61 (SEM), 32.40 ± 4.76 (p = 0.7), and 42.84 ± 1.91 (p = 0.0002).

(H–J) Transmission electron micrographs of wild-type, *Sdc*^{P}*/Df48,ubi-sara*, and *dlp*^{1}*/dlp*^{2} mutants show no gross ultrastructural morphology defects. Type 1b presynaptic boutons are surrounded by subsynaptic reticulum muscle membranes (SSR) and contain characteristic membranous organelles and vesicles. One active zone (with t bar) is marked in each micrograph with an asterisk. Inset in (H) shows a higher magnification view of a presynaptic mitochondrion as an indication of the quality of fixation and osmotic balance.

(K–M) Intermediate magnification of the presynaptic membrane shows multiple active zones (AZ) in the same genotypes. Arrowheads mark the AZ boundaries and t bar structures are marked with asterisks.

(N–P) High magnification views of AZs in the three genotypes reveal characteristic t bar structures (arrows) and proximal vesicle accumulations.

(Q) Bar graphs of mean AZ areas measured from serial reconstructions in wild-type, *Sdc*, and *dlp* mutants show a significant decrease in *dlp* mutants (p = 0.02; asterisk). The number of active zones reconstructed for each genotype were wild-type (n = 19), *Sdc*$^{I(2)10608}$*/Df(2R)48,ubi-sara* (n = 21), and *dlp*^{1}*/dlp*^{2} (n = 42). The number of boutons reconstructed for this analysis was: wild-type (n = 5), *Sdc*$^{I(2)10608}$*/Df(2R)48,ubi-sara* (n = 6), and *dlp*^{1}*/dlp*^{2} (n = 11).

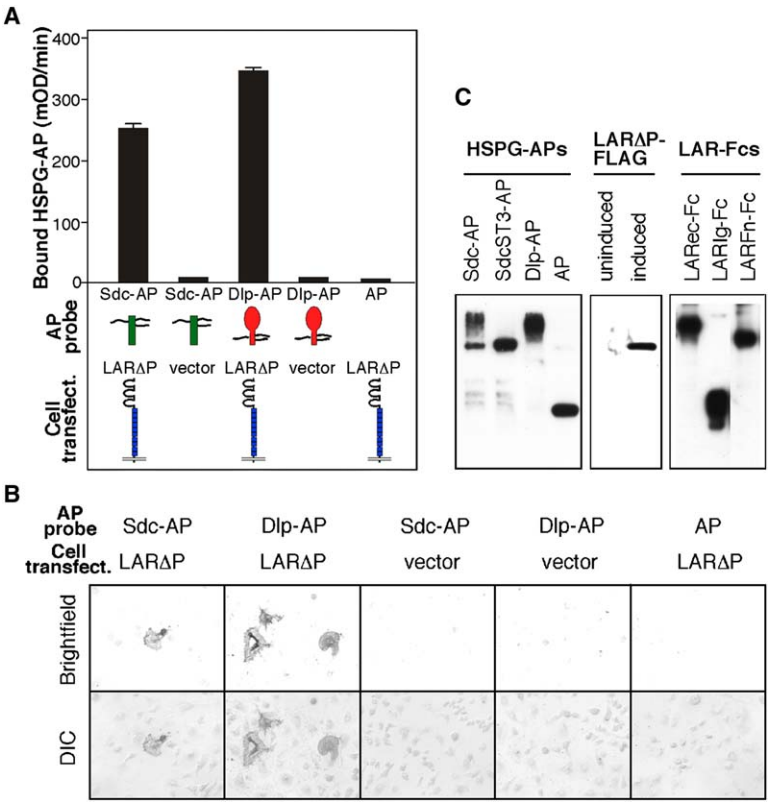

Figure 4. Sdc and Dlp Bind to Cell Surface LAR

(A) Quantification of Sdc-AP or Dlp-AP binding to LAR-transfected cells. Sdc-AP or Dlp-AP probes, or an AP control, were tested for binding to *Drosophila* S2 cells transfected with LARΔP-FLAG, a variant with the phosphatase domains deleted to avoid reduced cell viability, or to control cells transfected with empty vector. Both Dlp-AP and Sdc-AP showed little binding to control S2 cells and much stronger binding to cells transfected with the LAR construct LARΔP-FLAG ($p < 0.0001$). Dlp-AP bound to LAR transfected cells at higher levels than did Sdc-AP ($p < 0.001$). Bars represent mean ± SEM; performed in triplicate.

(B) Sdc-AP and Dlp-AP binding to LAR-transfected cells detected by in situ staining. Both Sdc-AP and Dlp-AP bound to LAR-transfected cells and showed cell-surface staining not seen in controls. Dlp-AP stained more cells with greater intensity than Sdc-AP. All images 20× magnification; top row are brightfield, and bottom row are DIC images.

(C) Western blotting (IB) of recombinant proteins. Left: AP fusion proteins detected by IB for a C-terminal myc tag. Sdc-AP appears as approximately 90 kDa, with a smear extending up to the wells (presumably HS-modified Sdc-AP). In contrast, ST3-AP, an Sdc variant with the HS attachment sites mutated, migrates as a single band at 90 kDa, without the higher molecular weight species, consistent with a lack of HS. Similar to Sdc-AP, Dlp-AP migrates as a smear from its calculated 137 kDa. Control unfused AP (approximately 67 kDa) is also shown. Middle: inducible LARΔP-FLAG expression in transfected S2 cells. Membrane fractions of uninduced and induced LAR-transfected cells were tested by IB for a C-terminal FLAG tag. The LARΔP-FLAG protein is detected as a band at the expected molecular weight. Right: expression of DLARec-Fc, DLARIg-Fc, or DLARFn-Fc detected at the expected molecular weights by IB for the C-terminal Fc tag.

LAR receptor (Figure 4C). Sdc-AP showed little binding to untransfected S2 cells but bound strongly to cells transfected with a LAR construct ($p < 0.0001$) (Figures 4A and 4B).

In view of this interaction between Sdc and LAR, we wondered if LAR might also associate with Dlp. Like Sdc-AP, Dlp-AP bound effectively to S2 cells in a LAR dependent fashion. In fact, in both quantitative assays (Figure 4A) and cell culture binding assays (Figure 4B), Dlp-AP consistently bound to LAR-transfected cells to a greater extent than did Sdc-AP ($p < 0.001$) (Figure 4A), suggesting that LAR might have a greater affinity for Dlp than for Sdc.

To confirm the binding of LAR with Sdc and Dlp in a cell-free system and to characterize the interaction in more detail, we used a quantitative in vitro protein binding assay in which Dlp-AP or Sdc-AP fusion proteins were tested for binding to a LAR-Fc fusion protein. Sdc-AP displayed saturable binding to LAR-Fc (Figure 5A). Scatchard analysis of the binding data revealed a dissociation constant (K_D) of approximately 13 nM for Sdc-LAR binding (Figure 5B).

To localize the binding region within LAR and within Sdc, we analyzed mutant proteins. Deletion mutants of LAR showed that Sdc associated specifically with the Ig but not the FN domains of the LAR extracellular domain (Figure 5E). A mutant Sdc-AP, in which all GAG attachment serine residues have been changed to threonines (ST3-AP), did not bind to LAR (Figure 5E). Moreover, heparitinase treatment of Sdc-AP to remove HS chains also abrogated LAR binding (Figure 5F). In contrast to vertebrate PTP-δ (Wang and Bixby, 1999), we were unable to detect homotypic binding of the *Drosophila* LAR ectodomain to itself in this assay (not shown).

Like Sdc, Dlp-AP showed high-affinity, saturable binding to recombinant LAR-Fc protein (Figure 5C) with a K_D of approximately 8 nM (Figure 5D). Interestingly, the affinity of Dlp for LAR was about twice as strong as that of Sdc in repeated experiments (Figure 5D and data not shown). Thus, the difference between Sdc and Dlp in the efficiency of their binding to the surface of LAR-transfected cells (Figure 4) might be explained solely by the difference between their K_D values (Figure 5). Like Sdc, Dlp-AP binding to LAR-Fc was specific

(R) A bar graph of the number of active zones per bouton reveals a substantial increase in *dlp* mutants.

(S) To test if Dlp is limiting for active zone dimensions, we used a postsynaptic GAL4 to express UAS-Dlp(+) in a wild-type background. 21 active zones were reconstructed, revealing a 1.6-fold increase in active zone area ($p = 0.009$; asterisk). Scale bar represents 600 nm in (H)–(J), 150 nm in (K)–(M), and 80 nm in (N)–(P).

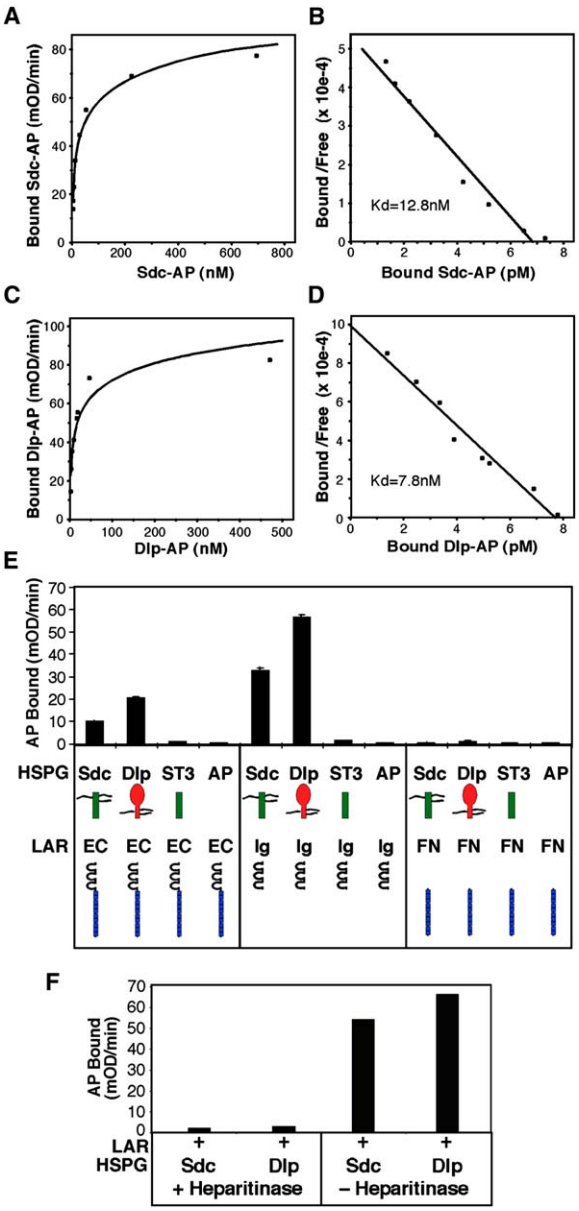

Figure 5. Syndecan and Dallylike Bind to LAR at High Affinity

(A and B) Saturation binding and Scatchard analysis of Sdc-AP binding to LAR-Fc.

(C and D) Saturation binding and Scatchard analysis of Dlp-AP binding to LAR-Fc. In each case, binding was saturable and produced an apparently linear Scatchard plot. The experiment shown gave K_D values of 12.8 nM and 7.8 nM for Sdc and Dlp respectively; similar values were obtained in repeated experiments, with Dlp-AP reproducibly showing a K_D approximately half that of Sdc-AP.

(E) Domain analysis of Sdc-AP and Dlp-AP binding to LAR-Fc. LARec-Fc, which includes the full LAR ectodomain, binds to Sdc-AP or Dlp-AP, but not to ST3-AP, a variant with the HS attachment sites mutated. Sdc-AP and Dlp-AP bound to LARIg-Fc, containing the Ig-like domains, but not to LARFn-Fc, containing the fibronectin-III type repeats. The HSPG binding domain therefore localizes to the Ig domains of LAR, and binding by Sdc-AP is dependent on HS chains.

(F) LAR binding by Sdc-AP and Dlp-AP is reduced by removal of HS chains. AP fusion proteins were pretreated with heparitinase and tested for LAR binding activity.

to the Ig domains and was highly sensitive to heparinase (Figures 5E and 5F).

Syndecan and LAR Act in a Common Genetic Pathway

The synapse growth phenotype that we discovered in *Sdc* mutants (Figure 2) is essentially identical to that observed in *LAR* mutants (Kaufmann et al., 2002). In addition, we find overlap between Sdc and LAR surrounding the presynaptic membrane (Figure 1H). These features, together with the biochemical association of Sdc and LAR (Figures 4 and 5), suggest that Sdc acts in the LAR pathway. If Sdc function relies upon LAR activity, we would predict that a reduction in LAR should enhance a weak *Sdc* phenotype. We introduced one null allele of *LAR* (*$LAR^{5.5}$*/+) into an *Sdc* hypomorphic background (*Sdc^{PKG}/Df48,ubi-sara*) and found that *LAR*/+ enhanced the NMJ growth defect of Sdc to a level approaching that of the *LAR* homozygote (Figure 6A).

A more stringent way to test if two genes act in the same pathway is to compare their single and double homozygous phenotypes. If Sdc and LAR act in independent parallel pathways, the two phenotypes should be additive. However, if they act in the same pathway, the double null should display the same phenotype as the single null. We used genetic recombination to combine null alleles of *Sdc* and *LAR* and found that the double mutant is indistinguishable from the *LAR* null alone (Figure 6B). Because Sdc is limiting for synapse growth in *Drosophila* (Figures 2K and 2L), we could demonstrate this in a complementary way by asking if LAR is absolutely required for Sdc to promote the addition of new boutons. We compared presynaptic elevation of Sdc in a wild-type background to the same expression in a *LAR* null background. Sdc gain of function in a *LAR* mutant background was identical to *LAR* alone (Figure 6B), showing that all of the Sdc growth-promoting activity is dependent on LAR.

Dallylike Opposes LAR Function

Although the synaptic localization and high affinity binding of Dlp and LAR suggested that Dlp might act in the LAR pathway, the active zone morphology and electrophysiology phenotypes of *dlp* and *LAR* mutants are opposite (Figure 3) (Kaufmann et al., 2002). This suggested that Dlp might act to antagonize synaptic LAR. If this were true, we reasoned that overexpression of Dlp might inhibit LAR function and thus phenocopy a *LAR* mutant. Using UAS-Dlp, we found significant decreases in bouton numbers with either presynaptic or postsynaptic GAL4 drivers, although a much stronger effect was seen from muscle expression (14% decrease with elav-GAL4 compared to 30% decrease with 24B-GAL4) (Figure 6D). Although this gain-of-function phenotype was similar to *LAR* LOF, satisfying our prediction, we further reasoned that an instructive upstream antagonist should be able to block the effect of LAR overexpression. Indeed, although overexpression of LAR alone increased bouton number, simultaneous elevation of Dlp and LAR gave a phenotype the same as Dlp alone (Figure 6E).

If LAR and Dlp were to act in separate parallel pathways, we would predict that Dlp overexpression combined with a *LAR* null would have additive effects in

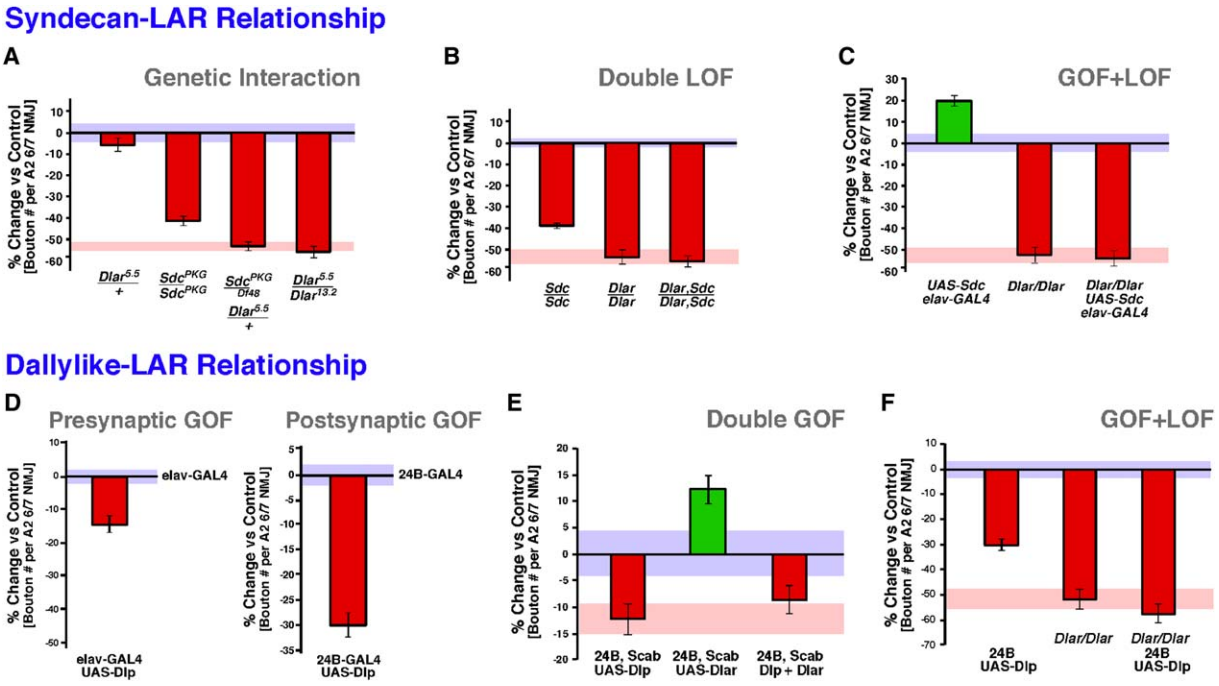

Figure 6. Syndecan and Dallylike Act in the LAR Pathway

(A–F) Double mutant assays score NMJ size in bouton number plotted as percentage change compared to a wild-type control. Green and red in the vertical bars represents increase and decrease relative to controls, respectively. Blue and pink horizontal bars represent SEM in wild-type and selected mutant, respectively. (A) Dose-dependent interaction between Sdc and LAR: a single allele of *LAR* (*Dlar*$^{5.5}$/+) crossed into a *Sdc* hypomorph (*Sdc*^{PKG}/*Df48, ubi-sara*) and compared to single mutants and LAR homozygotes for NMJ size. Reduction of *LAR* enhances the weak *Sdc* phenoytpe. (B) A double loss-of-function mutant lacking both Sdc and LAR is not significantly different in bouton number than a *LAR* null alone. (C) Presynaptic (elav-GAL4) elevation of UAS-Sdc increases bouton number relative to controls; however, Sdc displays no gain-of-function activity when combined with a Dlar null genetic background. (D) Presynaptic (elav-GAL4) or postsynaptic (24B-GAL4) elevation of UAS-Dlp induce a significant percentage decrease in bouton number at the A2 6/7 NMJ. (E) Using a combination of pre- and postsynaptic drivers (scabrous-GAL4+24B-GAL4), we find that Dlp and LAR have opposing effects on bouton number and that combined expression of Dlp and LAR decreases NMJ size. (F) Postsynaptic overexpression of Dlp causes a significant decrease in NMJ size, as does loss of LAR activity; however, the combined effects of both perturbations (GOF+LOF) are not significantly different than loss of LAR alone.

reducing NMJ size; however, if both genes function in the same pathway, the combined phenotype should be no stronger than the *LAR* null alone. We found the latter to be true, with no significant difference between *LAR*$^{13.2}$/*LAR*$^{5.5}$and *LAR*$^{13.2}$/*LAR*$^{5.5}$;*24B-GAL4/UAS-Dlp* (Figure 6F). Together, these gain-of-function assays support the hypothesis that Dlp antagonizes LAR in vivo.

Dallylike Acts Uptream of LAR to Regulate Tyrosine Phosphorylation

A direct way to show that Dlp regulates LAR receptor signaling activity is to assay the activation state of downstream effector proteins. In our previous analysis of LAR signaling, we discovered that the phosphoprotein Enabled (Ena): (1) displays a *LAR*-like axon phenotype, (2) binds directly to the LAR cytoplasmic domain, and (3) can be dephosphorylated by LAR (Wills et al., 1999). Our previous assays for LAR catalysis were performed in vitro, and so we wanted additional confirmation that Ena interacts with the LAR catalytic active site in an intact cell. For this purpose, we constructed active site point mutations that allow PTPs to bind phosphorylated substrates and initiate the first step of catalysis but then fail to release the bound substrate ("substrate trap") (Garton et al., 1996). Using wild-type and substrate trapping mutations (D-A in D1 and D2 PTP domains) in epitope-tagged LAR catalytic domains, we asked if endogenous Ena in *Drosophila* S2 or KC167 cells binds preferentially to either construct. As assayed by affinity purification and Western blot, Ena bound to the wild-type LAR PTP domains, with no binding to the tag alone (Figure 7A). However, the LAR substrate trap bound far more effectively to Ena under identical conditions (Figure 7A), supporting our previous genetic hypothesis that Ena is a physiological LAR substrate.

To provide a functional assay for LAR activity, we then used RNA interference (RNAi) in *Drosophila* KC167 cells followed by immunoprecipitation of endogenous Ena (Figure 7B). When we knocked down endogenous LAR and then assayed Ena by anti-phospho-tyrosine (p-Tyr) Western blot, we found a reproducible increase in Ena phosphorylation ($p = 0.016$) (Figures 7B and 7C), as predicted from our substrate-trapping data. When we used RNAi to reduce endogenous Dlp expression, we found the opposite effect on Ena phosphorylation ($p = 0.002$) (Figures 7B and 7C), consistent with a model in which Dlp acts to inhibit LAR activity. To test if Dlp acts upstream in a LAR-dependent fashion, we performed a double-RNAi of both proteins. Here, we found that the LAR phenotype was epistatic to Dlp (Figures 7B and 7C). This last experiment demonstrates that Dlp

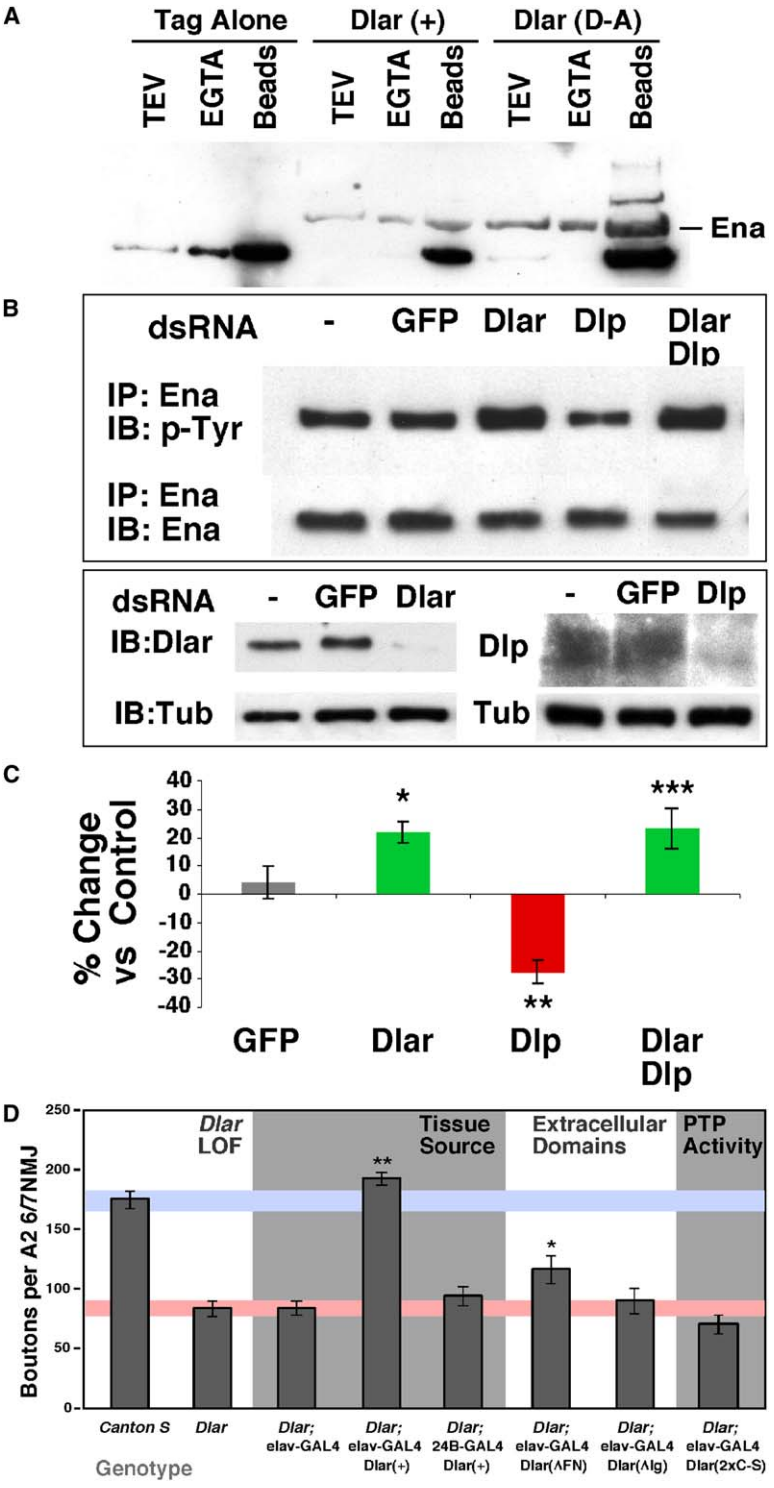

Figure 7. Dallylike and LAR Have Opposing Effects on Ena Phosphorylation

(A) Expression of epitope-tagged *Drosophila* LAR cytoplasmic domain constructs (Dlar D1+D2 PTP) in S2 cells followed by purification of either the tag alone, wild-type LAR (Dlar [+]), or a dual substrate trapping mutation in both PTP domains D1 and D2 (Dlar[D-A]) was used in combination with Western blot (IB) with anti-*Drosophila* Ena to assay for relative levels of Ena-LAR association. Endogenous Ena bound far more effectively to the LAR substrate trapping mutant. Parallel experiments were performed in KC167 cells with similar results.

(B) *Drosophila* KC167 cells were used for RNA interference targeting GFP (as a control), Dlar, and/or Dlp. Subsequent immunoprecipitation (IP) of endogenous Ena followed by Western blot (IB) with either anti-phosphotyrosine (p-Tyr) or anti-Ena (to normalize) assayed Ena phosphorylation. Control IB data are shown to document the level of Dlar and Dlp.

(C) Quantification of gel-band density from (B) shows the percentage change in Ena tyrosine phosphorylation compared to untreated controls after knock down of Dlar, Dlp, or both proteins (single asterisk, p = 0.016; double asterisk, p = 0.002; triple asterisk, p = 0.023).

(D) To assess the activity of *Drosophila* LAR (Dlar) UAS-cDNA transgenes during NMJ growth, we compared LAR null mutants ($Dlar^{13.2}/Dlar^{5.5}$) to a wild-type control (Canton S) and to lines expressing GAL4 in this background. Although neither GAL4 alone nor postsynaptic expression of a full-length, wild-type LAR (Dlar [+]) rescued the A2 6/7 NMJ phenotype, presynaptic LAR expression restored the mutant NMJ (asterisk). When transgenes lacking either the FN domains 2–9 (ΔFN), Ig domain 1–3 (ΔIg), or the two catalytic cysteine residues in PTP domains D1 and D2 (2xC-S) were assayed with elav-GAL4, only UAS-DlarΔFN provided significant rescue activity (p = 0.017; double asterisk).

acts upstream of LAR, supporting a model in which Dlp regulates Ena phosphorylation via inhibition of LAR activity.

Ig Domains and Catalytic Activity Are Essential for Synaptic LAR

A model in which Sdc and Dlp regulate LAR activity through direct binding would predict that the Ig domains and catalytic activity of the receptor be necessary for NMJ development. However, in a recent analysis of LAR domains required for rescue of lethality, we found that neither of these conserved features were absolutely required (Krueger et al., 2003). Thus, we wanted to re-examine this question in the context of the NMJ. Before testing different *LAR* mutant trangenes, we asked where full-length, wild-type LAR must be expressed to rescue

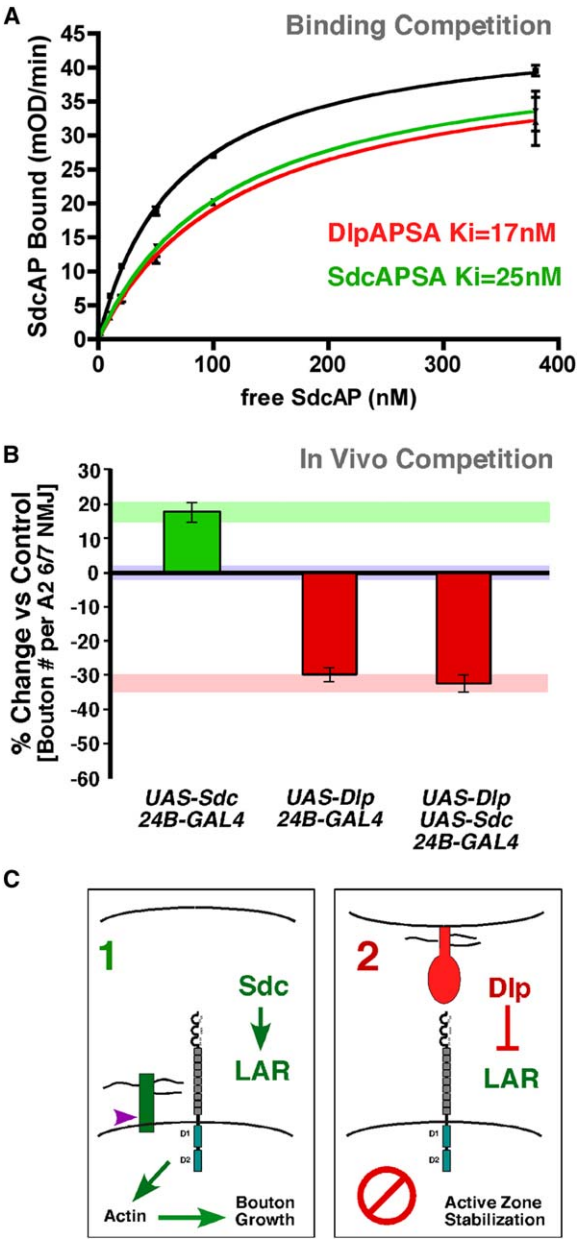

Figure 8. HSPG Competition for LAR Binding and Biological Activity

(A) Competition between Sdc and Dlp fusion proteins for binding to LAR in vitro. Sdc-AP was tested for binding to LAR-Fc, in the presence or absence of competing fusion proteins Dlp-AP^{SA} (red line) or Sdc-AP^{SA} (green line). The observed Bmax (maximal binding) of SdcAP to LAR was similar in each case (43.6, 41.8, and 42.3 mOD/min, respectively, in the presence of Dlp-AP^{SA}, Sdc-AP^{SA}, and control), indicative of competitive rather than noncompetitive binding inhibition. Dlp-AP^{SA} reproducibly showed a K_i lower than that of Sdc-AP^{SA}; the experiment shown here gave K_i values of approximately 25 nM and 17 nM for Sdc-AP^{SA} and Dlp-AP^{SA}, respectively, with similar values obtained in repeated experiments.

(B) Bouton number was quantified and plotted as percentage change relative to control in larvae overexpressing either Sdc, Dlp, or both under control of 24B-GAL4 to determine which HSPG is dominant in vivo. UAS-Dlp alone was indistinguishable from UAS-Dlp+UAS-Sdc. Light green, blue, and pink horizontal bars represent SEM for UAS-Sdc, 24B-GAL4 control, and UAS-Dlp+UAS-Sdc, respectively.

(C) Based on genetic data, LAR functions presynaptically to link bouton growth and active zone formation. Sdc (green) functions with LAR to promote bouton growth (1), a function dependent on LAR catalytic activity. Dlp (red) inhibits LAR activity (2) and is required to regulate active zone formation, presumably by blocking growth signals in favor of other effectors. Biochemical and genetic data suggest that Dlp has a competitive advantage. This leads to a model in which LAR mediates a natural transition between synapse growth and active zone assembly (step 1 to step 2).

a *LAR* null NMJ phenotype (see Experimental Procedures). Although muscle expression of UAS-LAR(+) with the GAL4 driver 24B did not rescue the *LAR* mutant phenotype, neuron-specific expression with elav-GAL4 restored *LAR* NMJs to normal size (Figure 7D, double asterisk). We then expressed three mutant transgenes of *LAR* under the same elav-GAL4 driver in the null background: ΔIg (removing all three Ig domains), ΔFN (removing FN repeats 2–9), and 2×C-S (eliminating catalytic activity in both PTP domains). However, at the NMJ only ΔFN provided any significant rescue activity compared to the *LAR* null alone ($p = 0.017$) (Figure 7D, single asterisk), demonstrating that LAR Ig domains and PTP catalysis are essential for synapse growth, as predicted by the biochemical and genetic data linking Sdc and Dlp to LAR function.

HSPG Competition for LAR Binding and Synapse Growth

Multiple experiments suggest that Sdc and Dlp exert opposing effects on LAR during synapse development. Because Sdc and Dlp are both present at the NMJ, this raised questions of whether the two HSPGs compete for access to LAR and which HSPG is dominant for binding and biological activity.

We first asked if the HSPGs can effectively compete with each other for binding to the LAR receptor. To produce a generally applicable vector for use in competition binding experiments with AP-tagged proteins, we constructed a version of the AP tag lacking catalytic activity. This construct was produced from the APtag-5 vector (Flanagan et al., 2000) by mutating Ser109 at the enzyme active site to Alanine, producing vector APtag-5^{SA}. Competition binding experiments were then performed by quantifying the bound AP activity after treating immobilized Fc-tagged LAR with AP-tagged HSPG, in the presence or absence of competing AP^{SA}-tagged proteins. The results show that Sdc and Dlp fusion proteins can compete with one another for binding to LAR-Fc (Figure 8A). Dlp-AP^{SA} gave more effective inhibition of binding, with a K_i value lower than that of Sdc-AP^{SA} (Figure 8A). The observed Bmax (maximal amount bound) for SdcAP was similar in the presence or absence of Sdc-AP^{SA} or Dlp-AP^{SA}, indicative of competitive rather than noncompetitive binding inhibition (Figure 8A and legend). A simple molecular interpretation would be that Sdc and Dlp bind to identical or overlapping binding sites on LAR.

Having shown that Sdc and Dlp compete for LAR binding in vitro and display opposite gain-of-function phenotypes during synapse development in vivo, we then asked if simultaneous elevation of the two genes would reveal which HSPG is dominant in vivo. Thus, we simultaneously elevated both Sdc and Dlp under a single GAL4 driver in a wild-type background and compared the outcome to expression of the single

transgenes under the same driver. We found that coexpression of Sdc and Dlp was indistinguishable from expression of Dlp alone (Figure 8B). This demonstrates that Dlp is completely dominant in vivo, consistent with the competitive advantage of Dlp over Sdc for LAR binding in vitro.

Discussion

Converging lines of evidence suggest that membrane-associated HSPGs serve an important purpose in the assembly, function and plasticity of excitatory synapses (reviewed by Van Vactor et al. [2006] and Yamaguchi [2001]). Here, we demonstrate that the ancient HSPG families of syndecans and glypicans are necessary for *Drosophila* to regulate distinct aspects of synaptic morphogenesis. Moreover, our genetic and biochemical data indicate that Sdc and Dlp interact with a shared receptor (LAR) to control presynaptic properties. Because LAR-family RPTPs have been shown to control the formation of excitatory synapses in *Drosophila*, *C. elegans*, and mammals (Ackley et al., 2005; Dunah et al., 2005; Kaufmann et al., 2002), our findings may represent a more general mechanism for regulating synaptic morphogenesis and function. Despite the importance of LAR-family RPTPs during cellular morphogenesis inside and outside of the nervous system (reviewed by Johnson and Van Vactor [2003]), the lack of physiologically relevant extracellular binding partners has made it challenging to study this well-conserved group of receptors.

Syndecan and LAR Promote Synaptic Growth

Our data show that Sdc promotes the formation of presynaptic boutons. This Sdc function appears to be mediated by LAR, as supported by parallel phenotypes, direct binding, in vivo colocalization, and three types of double mutant analysis between Sdc and LAR. Despite the fact that Sdc exhibits gain-of-function activity and endogenous expression on both sides of the synapse, our neuronal and muscle-specific rescue experiments show that Sdc function is mainly presynaptic. Because LAR is required only in neurons to promote synapse growth, our findings support a model in which Sdc acts as a neuronal cell-autonomous agonist of LAR. This is somewhat surprising, given the fact that soluble forms of Sdc bind to LAR and that endogenous Sdc appears to be released from the presynaptic membrane to fill the SSR. One way for Sdc to act presynaptically would be to bind to LAR even before the two proteins are presented on the neuronal surface. Because Dlp has a competitive advantage over Sdc for binding to LAR, a prebound complex of Sdc and LAR would have the ability to stimulate synapse growth before the phosphatase could be inhibited by Dlp. Such a mechanism could provide a time- and/or HSPG concentration-dependent switch from bouton addition to active zone assembly (Figure 8C).

Sdc could promote LAR activity in collaboration with an additional cell-type-specific membrane protein. Data from a parallel study also identified Sdc-LAR interactions during embryonic motor axon guidance (Fox and Zinn, 2005). However, in contrast to CNS pathfinding (Johnson et al., 2004; Steigemann et al., 2004), complete loss of Sdc alone has no significant effect on motor pathfinding (Fox and Zinn, 2005; this study), suggesting that additional LAR ligands exist in the early embryo. Recent experiments with the vertebrate LAR ortholog PTP-σ suggest that non-HSPG ligands may regulate its ability to promote retinal axon outgrowth (Sajnani et al., 2005). Although it remains a formal possibility, an additional ligand may not be needed to account for the NMJ growth-promoting activity of LAR because the larval synaptic phenotype in *Sdc* mutants is nearly as strong as the growth defect in *LAR* mutants (Figure 2) (Kaufmann et al., 2002).

Dallylike and LAR Interact to Control Active Zone Form and Function

Active zone assembly is vital for neurotransmission at the synapse and has been proposed as a means to modulate synaptic function over time (reviewed by Zhai and Bellen [2004]). Our analysis of Dlp reveals that synaptic glypicans are required to regulate active zone morphology and function. Moreover, we find that Dlp is limiting for active zone morphogenesis, consistent with an instructive role. Because the activities of Dlp appear opposite to those of LAR, we propose that the high affinity binding of Dlp to LAR induces an inhibition of receptor function (Figure 8C). This hypothesis is supported by the double RNAi experiments showing that the LAR effect on Ena phosphorylation is epistatic to the effect of Dlp, indicating that Dlp acts upstream of LAR. Because loss of Dlp at the NMJ did not induce a significant change in the number of presynaptic boutons, the results lead to a model in which Dlp is specialized for control of active zone properties. Such a function might provide a means to independently regulate and spatially distinguish LAR inhibition from LAR activation. In any case, the presence of active zone phenotypes in *dlp* but not in *Sdc* reveals specialization among synaptic HSPGs.

LAR regulates both NMJ growth and active zone morphogenesis (Kaufmann et al., 2002). Thus, LAR appears to provide a link between two important synaptic properties that are regulated by different extracellular factors. A mechanism to couple bouton growth and active zone formation would make sense because active zones appear early in the nascent bouton (Zito et al., 1999). Because LAR catalytic activity is necessary for bouton addition, and yet LAR inhibition by Dlp appears necessary for proper active zone formation, LAR's role at the active zone may be primarily structural. For example, LAR may simply provide an anchorage point for synaptic components like the scaffolding protein Liprin-α that regulates active zone formation (e.g., Kaufmann et al. [2002]). Alternatively, LAR may exist in distinct yet active signaling states, one of which is dependent on PTP activity (promoting synapse growth), and one of which is dependent on recruitment of signaling molecules (controlling active zone assembly). Because loss of Dlp or LAR has opposite effects on quantal content at the NMJ, it is attractive to speculate that the Dlp-LAR pathway normally provides a means to modulate the strength of neurotransmission, either during NMJ growth or during synaptic plasticity. LAR PTPs are required for normal physiology and plasticity at mammalian hippocampal synapses (Dunah et al., 2005; Uetani et al., 2000).

HSPG Specificity at the Neuromuscular Junction

Sdc and Dlp are both HSPGs that bind to LAR and thus might be expected to act similarly, but our results show that their functions are different. One way to account for the specificity might be a difference in the effect of soluble versus cell-surface HSPGs on LAR. Some ligand molecules such as Ephrins function when clustered at high density (e.g., on a membrane surface) but fail to activate their receptors when presented in a soluble, monomeric form (reviewed by Flanagan and Vanderhaeghen [1998]). Another possibility could be that LAR binding or signaling is differentially influenced by direct protein-protein interactions with the Sdc versus Dlp core proteins. The two HSPGs have very different core structures; Sdc is a transmembrane molecule with HS modification sites near the N terminus, whereas Dlp is a GPI-anchored protein with HS sites proximal to the membrane and a large disulphide bonded globular domain located more distally (reviewed by Bernfield et al. [1999]). It may also be relevant that Dlp consistently bound more effectively to LAR than Sdc, with K_D measurements in solution showing an affinity approximately 2-fold higher. These results suggest a competition model in which Dlp displaces Sdc, possibly to favor the stabilization of active zones after new growth at the synapse. In this model, presynaptic growth would be initially promoted by Sdc and would then be limited or halted by Dlp binding after formation of close membrane contact between the nerve and muscle. Such a mechanism could insure a transition from growth to synapse stabilization (Figure 8C) and could participate in subsequent maintenance or plasticity of the synapse.

Of course other molecules influence synapse size, and these might include coligands or coreceptors that may bind to Sdc, Dlp, and/or LAR. Potential candidates might include bone morphogenic protein (BMP), the type II BMP receptor Wishful thinking (Wit), or the Wnt ortholog Wingless (Wg), which have all been shown to regulate NMJ morphology in *Drosophila* (Aberle et al., 2002; Marques et al., 2002; McCabe et al., 2003; Packard et al., 2002). However, in addition to significant phenotypic differences compared to the HSPGs, overexpression studies indicate that neither BMP nor Wg are limiting for NMJ morphogenesis (Aberle et al., 2002; Packard et al., 2002). In contrast, Sdc and Dlp are both limiting for different aspects of synapse development, consistent with an instructive role in this context. Consistent with this notion, Syndecan-2 is sufficient to promote dendritic spine maturation during hippocampal synaptogenesis in culture (Ethell and Yamaguchi, 1999). Although vertebrate Syndecan-2 has yet to be tested at the synapse by loss of function, the colocalization and parallel biology of Synecan-2 and vertebrate LAR-family receptors strongly suggest conservation in the regulation of synaptic LAR (Dunah et al., 2005; Hsueh and Sheng, 1999; Hsueh et al., 1998).

Conclusions

The genetic and biochemical studies described here identify a partnership between HSPGs and LAR in *Drosophila* NMJ development that sets precedents for (1) the in vivo requirement for members of the syndecan and glypican families in synapse growth and electrophysiological function, (2) the specificity of HSPG function at the synapse, with distinct actions of Sdc and Dlp, and (3) biochemical identification of Sdc and Dlp as LAR binding partners, plus genetic evidence to place them in a pathway regulating biological function at the synapse.

Experimental Procedures

Genetics

Drosophila strains descrbed in Baeg et al. (2001), Han et al. (2004), Johnson et al. (2004), Kaufmann et al. (2002), Kirkpatrick et al. (2004), and Luo et al. (1994) were balanced over CyO-[actin-GFP], whereas *dlp* alleles were balanced over Tm6B-[ubi-GFP].

Immunohistochemistry of Cells and Tissues

Wandering third instar larvae from sparsely populated bottles were collected and dissected in Ca^{2+}-free saline. Several antibodies required a detergent-free protocol to visualize labeling at the NMJ, including anti-Dlar (1:100; gift from H. Saito), anti-Sdc (1:250) (Spring et al., 1994), and anti-Dlp (1:50) (Lum et al., 2003). Other antibodies (anti-Futsch [1:50] [Roos et al., 2000], mAb GluRIII [1:5000; gift from A. DiAntonio], anti-HRP [1:2000; Capell], anti-FasII [1:20] [Van Vactor et al., 1993], NC82 [1:100; gift from A. Hofbauer], anti-Dlg [1:1000; gift from V. Budnik], anti-Cysteine string protein [CSP; 1:1000], and anti-Synaptotagmin anti-Endophilin [Syt; 1:1000 and 1:500; gifts from H. Bellen]) were used as previously described (Kaufmann et al., 2002). Statistical analysis of boutons per NMJ was conducted in Excel by Student's t-test. Confocal microscopy was performed as described (Johnson et al., 2004).

Fusion Proteins and Binding Assays

AP fusion constructs were generated by inserting ectodomain sequences for Sdc or Dlp in APtag5 (Flanagan et al., 2000). Fc fusion proteins were in the Ig2eco vector (Cheng and Flanagan, 2001), and Fc fusion concentration was normalized by Western blot against the human Fc tag (see below). LARΔP-FLAG was generated by amplifying the ectodomain and transmembrane domains of LAR with PCR and subcloning into pMTAV5His. The three serine attachment sites were converted to threonine (ST3) to remove the glycosylation sites on Syndecan. Ser109 of APtag-5 was changed to alanine by PCR, generating AP^{SA} to create a catalytically-inactive AP for competition experiments.

Cell-free binding assays were performed with Reacti-Bind Protein A-coated microtitre plates (Pierce). Wells were blocked with HBAH (Hank's Buffered Saline Solution with 0.5 mg/ml BSA and 20 mM Hepes 7.0) for 15 min. DLAR-Fc fusion protein conditioned media (approximately 2 μg/ml) were allowed to bind to protein A for 1.5 hr, room temperature. Wells were then washed four times with HBAH, treated with AP fusion-conditioned medium for 1.5 hr, and then washed and assayed for bound AP activity as described (Flanagan et al., 2000). For heparitinase treatment, 200 μl of 30 nM AP fusion protein was incubated with 5 mU heparitinase (Seikagaku) or mock treated at 37ºC for 1 hr. The concentration of the "cold" HSPG-AP^{SA} fusion proteins used in competition binding experiments was approximately 25 nM as determined by comparison of HSPG-AP^{SA} and HSPG-AP conditioned media by Western blot. Cell surface binding assays were performed as described (Flanagan et al., 2000) by using S2 cells transfected with Fugene (Roche) and grown in suspension or on ConA-treated coverslips.

Protein Sample Preparation, RNA Interference, and Western Blotting

Transfected S2 cells were incubated in five volumes of hypotonic lysis buffer (25 mM Tris 7.5, 1 mM DTT, 1 Complete protease inhibitor tablet [Roche]) on ice for 10 min. Lysates were passed through a G27 syringe needle five times, and nuclei were pelleted (5000 RPM, 4ºC, 5 min). The supernatants (membrane fractions) were collected and pelleted (12,000 RPM, 4ºC, 10 min). Pellets were resuspended in 200 μl 1× SDS/PAGE sample buffer.

For Western blot analysis of recombinant protein expression, fusion-protein-conditioned media or S2 cell membrane fractions were subjected to SDS/PAGE on a 9% gel, transferred to Hybond N+ membrane (AP fusion proteins) or PVDF membrane (Fc fusion proteins and S2 cell membrane fractions), and blocked in 4% milk/

TBST for 1 hr. Blots were incubated with primary antibodies overnight at 4ºC, and diluted 1:1000 in 4%milk/TBST: anti-Myc (9E10, Santa Cruz Biotech), anti-human Fc-HRP (Amersham), anti-FLAG (M2 mouse monoclonal, Sigma). Myc/Flag blots were washed five times in TBST and incubated with anti-mouse Fc-HRP (Amersham) 1:1000 in 4%milk/TBST 1 hr. Blots were washed five times in TBST and detected with ECL Plus reagent (Amersham).

Tandem affinity purification (TAP) was modified from Veraksa et al. (2005) (see Supplemental Data). RNA interference was modified from Worby et al. (2001) (see Supplemental Data). On completion of dsRNA treatment, cells were harvested, lysed (lysis buffer same as that used in TAP experiments described above), and an aliquot was used to assess the efficiency of the dsRNA treatment by electrophoresis on a 4%–15% gradient gel and immunoblotting with anti-Dlar (a kind gift of Kai Zinn, 1:100), anti-Dlp (DSHB, 1:1000), or anti-tubulin (Sigma, 1:3000) antibodies. For better resolution of Dlp, the lysate was treated with Heparinase III (Seikagaku) as described in Lum et al., 2003.

Ena monoclonal 1G6.C10 antibody was covalently attached to beads with the ProFound Coimmunoprecipitation kit (Pierce), followed by immunoprecipitation from control and dsRNA-treated Kc167 lysates described above by the manufacturer's protocol. After immunoprecipitation, samples were split in half, and electrophoretic separation on two 10% gels performed followed by immunoblotting with either the anti-Ena antibody or a cocktail (1:1 w/w) of rabbit polyclonal anti-phosphotyrosine antibodies (Upstate [06-427] and Chemicon [AB1599]) used at 2 μg/ml. Densitometric quantification was performed with the ImageJ software. Nitrocellulose membranes (Amersham) were used for all immunoblot experiment except for those involving detection of Dlp in which Hybond N+ membrane (Amersham) was used.

Electrophysiology

Electrophysiology was preformed on late third-instar larvae. Mutant larvae were raised on agar grape plates along with their heterozygous siblings and separated at early third instar. Larvae were dissected in Ca^{2+}-free HL-3 saline with the following ionic concentrations (in mM): 70 NaCl, 5 KCl, 20 $MgCl_2$, 10 NaHCO3, 5 trehalose, 115 sucrose, and 5 HEPES (pH 7.2) (Stewart et al., 1994). All recordings were measured in HL-3 saline containing 1 mM Ca^{2+}. Sharp microelectrodes (15–30 MOhms) were filled with 3 M KCl and were used to record membrane potentials from muscle six of abdominal segments A3 or A4. Wide bore suction electrodes were used to stimulate the segmental nerve, which was cut free from the ventral nerve cord. Spontaneous events were recorded in the absence of stimuli. Recordings were analyzed only if the resting membrane potential was ≤ -56 mV. Muscle input resistance was measured for each genotype and found to be similar to control. Data were collected with a Digidata1322A and Axopatch 2A amplifier (Axon Instruments). Evoked potentials were analyzed with Clampfit8.2 (Axon Instruments), and spontaneous events were analyzed with MiniAnalysis6 software (Synaptosoft, Inc.). The average EJP amplitude was calculated from averages of 20–25 events per each NMJ. 200 events per NMJ were averaged to calculate mini event amplitude while 3 min of recorded minis were used to calculate the mini frequency. Quantal content was corrected for nonlinear summation with the previously published method (McLachlan and Martin, 1981).

Electron Microscopy

Ultrastructural analysis was performed with modifications from (Kaufmann et al., 2002) (see Supplemental Data).

Supplemental Data

The Supplemental Data for this article can be found online at http://www.neuron.org/cgi/content/full/49/4/517/DC1/.

Acknowledgments

We are grateful to Dr. Michael Greenberg, Dr. Mark Emerson, and Miriam Osterfield for thoughtful discussions. We are grateful for Drs. Alexey Veraksa and Spyros Artavanis-Tsakonas for help with affinity purification methods. For *Drosophila* mutant strains, we thank Drs. Norbert Perrimon, Micheal O'Connor, and Scott Selleck and the Bloomington Drosophila Stock Center at the University of Indiana. For antibodies, we are grateful to Dr. Kai Zinn and Alois Hofbauer for unpublished antibodies and Drs. John Lincecum, Aaron DiAntonio, Dietmar Schmucker, Vivian Budnik, and Hugo Bellen for published reagents. We thank the Developmental Studies Hybridoma Bank (DSHB) at the University of Iowa, Department of Biological Sciences. We would also like to thank Dr. Jennifer Waters-Shuler and Lara Petrak at the Nikon Imaging Center at Harvard Medical School. D.V.V. is a Leukemia and Lymphoma Society Scholar and is supported by a grant from National Institute of Neurological Disorders and Stroke (NS40043). K.G.J. is supported by a postdoctoral fellowship from the Helen Hay Whitney foundation. J.G.F. is supported by a grant from NINDS (NS40043) as is T.L.S (NS41062). J.L.M. is supported by National Institutes of Health awards HD36081 and HD36049.

Received: August 18, 2005
Revised: December 7, 2005
Accepted: January 23, 2006
Published: February 15, 2006

References

Aberle, H., Haghighi, A.P., Fetter, R.D., McCabe, B.D., Magalhaes, T.R., and Goodman, C.S. (2002). *wishful thinking* encodes a BMP type II receptor that regulates synaptic growth in *Drosophila*. Neuron *33*, 545–558.

Ackley, B.D., Harrington, R.J., Hudson, M.L., Williams, L., Kenyon, C.J., Chisholm, A.D., and Jin, Y. (2005). The two isoforms of the *Caenorhabditis elegans* leukocyte-common antigen related receptor tyrosine phosphatase PTP-3 function independently in axon guidance and synapse formation. J. Neurosci. *25*, 7517–7528.

Aricescu, A.R., McKinnell, I.W., Halfter, W., and Stoker, A.W. (2002). Heparan sulfate proteoglycans are ligands for receptor protein tyrosine phosphatase sigma. Mol. Cell. Biol. *22*, 1881–1892.

Baeg, G.H., Lin, X., Khare, N., Baumgartner, S., and Perrimon, N. (2001). Heparan sulfate proteoglycans are critical for the organization of the extracellular distribution of Wingless. Development *128*, 87–94.

Bernfield, M., Gotte, M., Park, P.W., Reizes, O., Fitzgerald, M.L., Lincecum, J., and Zako, M. (1999). Functions of cell surface heparan sulfate proteoglycans. Annu. Rev. Biochem. *68*, 729–777.

Cheng, H.J., and Flanagan, J.G. (2001). Cloning and characterization of RTK ligands using receptor-alkaline phosphatase fusion proteins. Methods Mol. Biol. *124*, 313–334.

Dunah, A.W., Hueske, E., Wyszynski, M., Hoogenraad, C.C., Jaworski, J., Pak, D.T., Simonetta, A., Liu, G., and Sheng, M. (2005). LAR receptor protein tyrosine phosphatases in the development and maintenance of excitatory synapses. Nat. Neurosci. *8*, 458–467.

Ethell, I.M., and Yamaguchi, Y. (1999). Cell surface heparan sulfate proteoglycan syndecan-2 induces the maturation of dendritic spines in rat hippocampal neurons. J. Cell Biol. *144*, 575–586.

Flanagan, J.G., and Vanderhaeghen, P. (1998). The ephrins and Eph receptors in neural development. Annu. Rev. Neurosci. *21*, 309–345.

Flanagan, J.G., Cheng, H.J., Feldheim, D.A., Hattori, M., Lu, Q., and Vanderhaeghen, P. (2000). Alkaline phosphatase fusions of ligands or receptors as in situ probes for staining of cells, tissues, and embryos. Methods Enzymol. *327*, 19–35.

Fox, N.A., and Zinn, K. (2005). The heparan sulfate proteoglycan Syndecan is an in vivo ligand for the *Drosophila* LAR receptor tyrosine phosphatase. Curr. Biol. *15*, 1701–1711.

Garton, A.J., Flint, A.J., and Tonks, N.K. (1996). Identification of p130(cas) as a substrate for the cytosolic protein tyrosine phosphatase PTP-PEST. Mol. Cell. Biol. *16*, 6408–6418.

Gramates, L.S., and Budnik, V. (1999). Assembly and maturation of the *Drosophila* larval neuromuscular junction. Int. Rev. Neurobiol. *43*, 93–117.

Han, C., Belenkaya, T.Y., Wang, B., and Lin, X. (2004). *Drosophila* glypicans control the cell-to-cell movement of Hedgehog by a dynamin-independent process. Development *131*, 601–611.

Hsueh, Y.P., and Sheng, M. (1999). Regulated expression and subcellular localization of syndecan heparan sulfate proteoglycans

and the syndecan-binding protein CASK/LIN-2 during rat brain development. J. Neurosci. *19*, 7415–7425.

Hsueh, Y.P., Yang, F.C., Kharazia, V., Naisbitt, S., Cohen, A.R., Weinberg, R.J., and Sheng, M. (1998). Direct interaction of CASK/LIN-2 and syndecan heparan sulfate proteoglycan and their overlapping distribution in neuronal synapses. J. Cell Biol. *142*, 139–151.

Johnson, K.G., and Van Vactor, D. (2003). Receptor protein tyrosine phosphatases in nervous system development. Physiol. Rev. *83*, 1–24.

Johnson, K.G., Ghose, A., Epstein, E., Lincecum, J., O'Connor, M.B., and Van Vactor, D. (2004). Axonal heparan sulfate proteoglycans regulate the distribution and efficiency of the repellent slit during midline axon guidance. Curr. Biol. *14*, 499–504.

Kaufmann, N., DeProto, J., Ranjan, R., Wan, H., and Van Vactor, D. (2002). *Drosophila* liprin-alpha and the receptor phosphatase Dlar control synapse morphogenesis. Neuron *34*, 27–38.

Kirkpatrick, C.A., Dimitroff, B.D., Rawson, J.M., and Selleck, S.B. (2004). Spatial regulation of Wingless morphogen distribution and signaling by Dally-like protein. Dev. Cell *7*, 513–523.

Krueger, N.X., Reddy, R.S., Johnson, K., Bateman, J., Kaufmann, N., Scalice, D., Van Vactor, D., and Saito, H. (2003). Functions of the ectodomain and cytoplasmic tyrosine phosphatase domains of receptor protein tyrosine phosphatase Dlar in vivo. Mol. Cell. Biol. *23*, 6909–6921.

Lauri, S.E., Kaukinen, S., Kinnunen, T., Ylinen, A., Imai, S., Kaila, K., Taira, T., and Rauvala, H. (1999). Regulatory role and molecular interactions of a cell-surface heparan sulfate proteoglycan (N-syndecan) in hippocampal long-term potentiation. J. Neurosci. *19*, 1226–1235.

Luo, L., Liao, Y.J., Jan, L.Y., and Jan, Y.N. (1994). Distinct morphogenetic functions of similar small GTPases: *Drosophila* Drac1 is involved in axonal outgrowth and myoblast fusion. Genes Dev. *8*, 1787–1802.

Lum, L., Yao, S., Mozer, B., Rovescalli, A., Von Kessler, D., Nirenberg, M., and Beachy, P.A. (2003). Identification of Hedgehog pathway components by RNAi in *Drosophila* cultured cells. Science *299*, 2039–2045.

Marques, G., Bao, H., Haerry, T.E., Shimell, M.J., Duchek, P., Zhang, B., and O'Connor, M.B. (2002). The *Drosophila* BMP type II receptor Wishful Thinking regulates neuromuscular synapse morphology and function. Neuron *33*, 529–543.

McCabe, B.D., Marques, G., Haghighi, A.P., Fetter, R.D., Crotty, M.L., Haerry, T.E., Goodman, C.S., and O'Connor, M.B. (2003). The BMP homolog Gbb provides a retrograde signal that regulates synaptic growth at the *Drosophila* neuromuscular junction. Neuron *39*, 241–254.

McLachlan, E.M., and Martin, A.R. (1981). Non-linear summation of end-plate potentials in the frog and mouse. J. Physiol. *311*, 307–324.

Packard, M., Koo, E.S., Gorczyca, M., Sharpe, J., Cumberledge, S., and Budnik, V. (2002). The *Drosophila* Wnt, wingless, provides an essential signal for pre- and postsynaptic differentiation. Cell *111*, 319–330.

Rawson, J.M., Dimitroff, B., Johnson, K.G., Rawson, J.M., Ge, X., Van Vactor, D., and Selleck, S.B. (2005). The heparan sulfate proteoglycans Dally-like and Syndecan have distinct functions in axon guidance and visual-system assembly in *Drosophila*. Curr. Biol. *15*, 833–838.

Roos, J., Hummel, T., Ng, N., Klambt, C., and Davis, G.W. (2000). *Drosophila* Futsch regulates synaptic microtubule organization and is necessary for synaptic growth. Neuron *26*, 371–382.

Sajnani, G., Aricescu, A.R., Jones, E.Y., Gallagher, J., Alete, D., and Stoker, A. (2005). PTPsigma promotes retinal neurite outgrowth non-cell-autonomously. J. Neurobiol. *65*, 59–71.

Spring, J., Paine-Saunders, S.E., Hynes, R.O., and Bernfield, M. (1994). *Drosophila* syndecan: conservation of a cell-surface heparan sulfate proteoglycan. Proc. Natl. Acad. Sci. USA *91*, 3334–3338.

Steigemann, P., Molitor, A., Fellert, S., Jackle, H., and Vorbruggen, G. (2004). Heparan sulfate proteoglycan syndecan promotes axonal and myotube guidance by slit/robo signaling. Curr. Biol. *14*, 225–230.

Stewart, B.A., Atwood, H.L., Renger, J.J., Wang, J., and Wu, C.F. (1994). Improved stability of *Drosophila* larval neuromuscular preparations in haemolymph-like physiological solutions. J. Comp. Physiol. [A] *175*, 179–191.

Uetani, N., Kato, K., Ogura, H., Mizuno, K., Kawano, K., Mikoshiba, K., Yakura, H., Asano, M., and Iwakura, Y. (2000). Impaired learning with enhanced hippocampal long-term potentiation in PTPdelta-deficient mice. EMBO J. *19*, 2775–2785.

Van Vactor, D., Sink, H., Fambrough, D., Tsoo, R., and Goodman, C.S. (1993). Genes that control neuromuscular specificity in *Drosophila*. Cell *73*, 1137–1153.

Van Vactor, D., Wall, D.P., and Johnson, K.G. (2006). Heparan sulfate proteoglycans and the emergence of neuronal connectivity. Curr. Opin. Neurobiol., in press. Published online January 18, 2006. 10.1016/j.conb.2006.01.011.

Veraksa, A., Bauer, A., and Artavanis-Tsakonas, S. (2005). Analyzing protein complexes in *Drosophila* with tandem affinity purification-mass spectrometry. Dev. Dyn. *3*, 827–834.

Wang, J., and Bixby, J.L. (1999). Receptor tyrosine phosphatase-delta is a homophilic, neurite-promoting cell adhesion molecular for CNS neurons. Mol. Cell. Neurosci. *14*, 370–384.

Wills, Z., Bateman, J., Korey, C.A., Comer, A., and Van Vactor, D. (1999). The tyrosine kinase Abl and its substrate enabled collaborate with the receptor phosphatase Dlar to control motor axon guidance. Neuron *22*, 301–312.

Worby, C.A., Simonson-Leff, N., and Dixon, J.E. (2001). RNA interference of gene expression (RNAi) in cultured *Drosophila* cells. Sci. STKE *95*, PL1.

Yamagata, M., Sanes, J.R., and Weiner, J.A. (2003). Synaptic adhesion molecules. Curr. Opin. Cell Biol. *15*, 621–632.

Yamaguchi, Y. (2001). Heparan sulfate proteoglycans in the nervous system: their diverse roles in neurogenesis, axon guidance, and synaptogenesis. Semin. Cell Dev. Biol. *12*, 99–106.

Zhai, R.G., and Bellen, H.J. (2004). The architecture of the active zone in the presynaptic nerve terminal. Physiology (Bethesda) *19*, 262–270.

Zito, K., Parnas, D., Fetter, R.D., Isacoff, E.Y., and Goodman, C.S. (1999). Watching a synapse grow: noninvasive confocal imaging of synaptic growth in *Drosophila*. Neuron *22*, 719–729.